Atmospheric Environment 239 (2020) 117806

Contents lists available at ScienceDirect

Atmospheric Environment

journal homepage: http://www.elsevier.com/locate/atmosenv

Impact of a massive dust storm on the gross alpha, gross beta, ^{40}K, ^{137}Cs, ^{210}Pb, ^{7}Be activities measured in atmospheric aerosols collected in Tenerife, Canary Islands

María López-Pérez [a], José Miguel Lorenzo-Salazar [a], Francisco Javier Expósito [b], Juan Pedro Díaz [b], Pedro Salazar [a,c,*]

[a] Laboratorio de Física Médica y Radioactividad Ambiental, SEGAI, Universidad de La Laguna, Spain
[b] Grupo de Observación de La Tierra y La Atmósfera, Universidad de La Laguna, Spain
[c] Departamento de Medicina Física y Farmacología, Universidad de La Laguna, Spain

HIGHLIGHTS

- On February 2020, an intense dust storm struck the Canary Islands archipelago.
- PM10 air concentration reached levels of >3000 μg m^{-3}.
- Gross alpha, ^{137}Cs and ^{40}K showed higher values during such a dust storm.
- PCA identified two main components that explain 81% of the total variance.
- Three clusters are identified with Oceanic, Continental and Saharan origins.

GRAPHICAL ABSTRACT

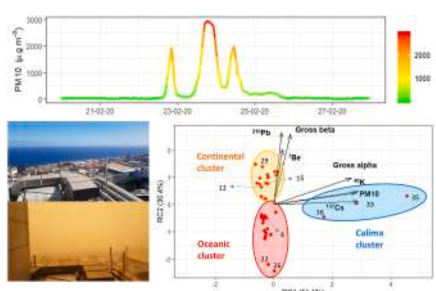

ARTICLE INFO

Keywords:
Dust storm
Aerosols
Atmospheric radionuclides
PM10
Back-trajectories

ABSTRACT

From February 22 to 24, 2020, an intense dust storm affected the Spanish archipelago of the Canary Islands. Here we assess the radiological impact on the Canary Islands population of several natural and artificial radionuclides (^{40}K, ^{137}Cs, ^{210}Pb, ^{7}Be), and other radiological parameters (gross alpha and gross beta activity concentrations) measured in atmospheric aerosols before, during and after the dust storm.

Total Suspended Matter highly correlated with PM10 (Pearson's correlation coefficient, $r_o = 0.98$), showed increments ranging from 849% to 1778% against the background average levels, reaching levels of >3000 μg m^{-3}.

^{40}K and ^{137}Cs radionuclides showed activity values over the minimum detection activity from January to March 2020, coupled with dust intrusion episodes during the study. This finding supports the use of these radionuclides as radiotracers for African low altitude dust intrusions occurring particularly during winter months over the Canary Islands.

A high correlation between gross beta and ^{210}Pb activities suggests that the latter is the main source for gross beta emitters in aerosol samples collected in the study region. ^{210}Pb and ^{7}Be showed a moderate positive correlation and did not show any significant change during the storm, suggesting a similar dynamics of alpha and beta emitters in the low atmosphere.

* Corresponding author. Departamento de Medicina Física y Farmacología, Universidad de La Laguna, Spain.
E-mail address: psalazar@ull.edu.es (P. Salazar).

https://doi.org/10.1016/j.atmosenv.2020.117806
Received 6 May 2020; Received in revised form 14 July 2020; Accepted 21 July 2020
Available online 25 July 2020

A Principal Component Analysis of these observations showed two components representing a Saharan component (based on ^{40}K, ^{137}Cs, gross alpha, and PM10) and a heterogeneous component representing North Atlantic and Europe air masses (based on ^{7}Be, ^{210}Pb, and gross beta).

In addition, a K-means cluster analysis helped to disentangle the origin of air masses arriving at the archipelago. Three different clusters were identified: a continental cluster (based on gross beta, ^{210}Pb, and ^{7}Be activity concentrations); an oceanic cluster (with low values of PM10 air concentrations, gross beta, gross alpha, and ^{210}Pb, and ^{7}Be and ^{40}K activity concentrations), reflecting the Atlantic air contributions with lower radionuclide activity and microparticulate matter; and a dust intrusion cluster (with high PM10 values and ^{137}Cs, ^{40}K and gross alpha activity concentrations) representing dust intrusion episodes observed in Tenerife Island. These studies allow the detection and monitoring of radioactive elements, estimating the potential radiological risk to the population associated with mineral dust intrusions.

1. Introduction

Sea salt and suspended dust particles are the two natural sources that contribute the most to the production of atmospheric aerosol (Andreae and Rosenfeld, 2008; Beuck et al., 2011; Cardoso et al., 2018; Zhang et al., 2020) and it can affect climate and human health (Goudie, 2014; Karanasiou et al., 2012; Perez et al., 2012; Querol et al., 2019b; WHO, 2013). Dust storms and plumes are relevant to global climate change, nutrient deposition (N, P, Fe cycles) and ecosystem regulation (Krupke et al., 2015; Okin et al., 2011), scattering and absorption of solar radiation (Gehlot et al., 2015; Schweitzer et al., 2018), cloud formation (Weger et al., 2018). Such dust particles, under certain meteorological conditions, can be transported at long distances (Prospero, 1999; Prospero et al., 2002) and have an important effect on the health of the population nearby (Middleton, 2017). The Sahara Desert, with 9 million square kilometers, is the largest and active airborne dust source in the world and it is responsible for 50–70% of the global emissions (Huneeus et al., 2011). According to the European Community Air Quality Directive (2008/50/EC), any given place in the EU cannot exceed the annual average PM10 concentration limit of 40 $\mu g\, m^{-3}$, moreover, the daily PM10 value (50 $\mu g\, m^{-3}$) cannot exceed more than 35 times in a year (2008/50/EC, 2011; WHO, 2006). Nevertheless, in such a directive this threshold is not applied to natural atmospheric events such as particle inputs from desert areas, volcanic eruptions, or wildfires. In this sense, African mineral dust intrusions are the main source of natural atmospheric aerosols in the Canary Islands (located 100 km off the west coast of Morocco) and it is the main reason why PM10 limiting values are exceeded throughout the year (Baldasano et al., 2014; Querol et al., 2008, 2019a). The Saharan dust events are an important source of ^{137}Cs and other artificial radionuclides originated from French nuclear weapons tests performed in the Saharan desert in the 1960s or deposited after the Chernobyl accident (Baggoura et al., 1998; Hernández et al., 2005b; Masson et al., 2010).

The present work analyses the PM10 concentration, atmospheric conditions, and radiometric measurements from atmospheric aerosols collected before, during, and after the occurrence of the dust outbreak on 22, 23, and 24 of February 2020 in the Canary Islands. This study allows us to evaluate the radiological impact on the Canary Islands population of several natural and artificial radionuclides (^{40}K, ^{137}Cs, ^{210}Pb, ^{7}Be), and other radiological parameters (gross alpha and gross beta activity concentrations) in atmospheric aerosols sampled during this dust intrusion episode.

1.1. Study area

Tenerife is the island with the largest extension (2,034 km^2) and the highest altitude (3718 m) in the Canary Islands. As is the case with the rest of islands in the archipelago, it has a volcanic origin. Regarding its location, Tenerife is situated approximately 250 km west from the northwestern coast of Africa, between 28° 18′N–28° 35′N and 16° 07′W −16° 49′ W, see Fig. 1. About 62% of the air masses in the marine boundary layer (MBL) come from the North and Northwest Atlantic and, to a lesser extent, from Europe and the Mediterranean region (13%) and Northern Africa (25%) (Viana et al., 2002). Other authors have quantified the Northern Africa contribution around 15% (Alonso-Pérez et al., 2007) or 31% of days per year (Querol et al., 2019a). Similarly, to other subtropical regions, its lower atmosphere enjoys a solid stability and strong stratification (Díaz et al., 2019; Viana et al., 2002). A stable temperature inversion is observed most days restricting the air exchange between the upper and lower atmospheric layers (Bustos Cuevas, 1998; Torres et al., 2001). The thickness of the inversion layer varies from 358 m (winter months) and 563 m (summer months) (Torres et al., 2001). Besides, its average altitude is higher in winter (between 1360 and 1850 m) and lower in summer (between 770 and 1380 m). Above the inversion temperature layer, the air is warm and dry, and humid and chill below this layer. The meteorological features of the Canary Islands are dependent on the strength and position of the subtropical North-Northeast (NNE) Atlantic anticyclone. From January to March, low-level dust intrusions coming from Africa cause the interruption of the normal NNE trade winds at MBL for short periods of time (3–8 days duration), which is known in Canary Islands as “calima” (Alonso-Pérez et al., 2007; Goudie and Middleton, 2001; Rodríguez and Guerra, 2001). Under this situation, a direct transport of dust from the Sahara Desert to the Canary Islands is frequently observed. Depending on where the air masses circulate, they could sweep the radionuclides present in the soil from areas where the French nuclear weapons tests (NWT) were conducted. Some authors have focused on the study of the natural and artificial radionuclides in those areas (Baggoura et al., 1998; Danesi et al., 2008). They found concentrations of ^{226}Ra, ^{214}Bi, ^{228}Ac, ^{212}Pb, ^{214}Pb, ^{40}K, ^{137}Cs, ^{238}Pu and $^{239+240}Pu$ in many soil sites in Algeria (Baggoura et al., 1998). Special attention has received the study of ^{137}Cs activity levels after the NWT occurred at the “Gerboise” site (Algeria) in the 1960s. The highest concentration detected of this artificial radionuclide in soils was 41 ± 4 Bq m^{-2} dry mass, with an average value of 11.1 Bq m^{-2} (Baggoura et al., 1998). In addition other authors reported concentrations of $29{\cdot}10^3$ Bq kg^{-1} in small areas of the NWT sites (Danesi et al., 2008). During exceptional Saharan dust outbreaks, an increase in the activity levels of ^{137}Cs measured in the SW of France (Masson et al., 2010; Menut et al., 2009) or Canary Islands (Spain) (Hernández et al., 2005a) has been observed.

1.2. The dust storm of February 2020 over the Canary Islands

Between 22 and 24 February 2020, one of the biggest dust storms of this century struck the Canary Islands (Fig. 1). The origin of this situation was a cut-off low formed from the polar jet stream in the previous days. The position of this low in those days to the west of the Canary Islands and an anticyclonic situation at northern latitudes gave rise to strong winds from the east. Fig. 2 clearly shows the position of the cut-off low, the high-pressure area at North, and the direction and strength of the winds.

The winds generated by this storm peaked, on several occasions, over 120 km h^{-1}, having a considerable impact on the agricultural sector with important economic losses (El_Día, 2020). Due to the poor visibility, all airports across the Canary Islands were closed, affecting ca. 800 flights (cancelled or re-routed), and most of them stayed closed until February 24, 2020 (Euronews, 2020; The_Washington_Post, 2020). Schools, universities, and local gathering events (Carnival) were cancelled, postponed or curtailed, and people were advised to stay at home with their windows closed due to the poor air quality. In addition, 2000 people were evacuated after strong winds whipped the flames from several wildfires on Gran Canaria and Tenerife islands, generating significant economic losses (El_Día, 2020). It worth mentioning that during that weekend four different emergency warnings were declared by the Government of the Canary Islands due to adverse environmental conditions (strong winds, high risk for wildfires, low visibility, and adverse coastal phenomenon) (El_País, 2020).

2. Sampling and method of analysis

Two air quality monitoring stations were used to collect aerosol samples for radiometric measurements, located within the Santa Cruz de Tenerife metropolitan area (FIMERALL stations; 28° 27′18″N; 16° 17′29′W, 295 m.a.s.l.). In order to collect Total Suspended Particulates (TSP) at a height of 1 m above the ground level, two separate aerosol sampling pumps, a Saic Radecco AVS-28A (low-flow station) and a Physik Technic Innovation ASS-500 (high-flow station), were used.

Airflow rates, at normal conditions, were 35 and 11,500 $L\,min^{-1}$, respectively. Circular cellulose (0.47 cm diameter) and polypropylene square (44 × 44 cm^2) filters (Fig. 3) were used for the low-flow and high-flow stations, respectively. The radionuclide aerosol collection efficiency is 93–94% for the polypropylene filter and 100% for particles larger than 0.8 μm in the cellulose filter. The filters were exchanged weekly. The cellulose filters were used to determine gross alpha and gross beta activity concentrations, and the polypropylene one to analyze gamma-emitting radionuclides. The location and positioning of the stations/pumps were chosen to minimize the contamination of the filters by re-suspension of local soil particles.

TSP matter deposited in the filter was calculated gravimetrically by weighing the filters with a precision balance before and after exposure. The filter of the high-flow station was introduced in a plastic box and kept in a desiccator, and measured 3 days after preparation. The cellulose filter was placed in a 0.5 cm diameter stainless steel planchet until measurement.

Low-level high-resolution gamma spectrometry with coaxial-type germanium detectors (Canberra Industries Inc., USA) was used to perform gamma measurements with a relative efficiency of 20% and a resolution of 1.9 KeV for the 1333 KeV ^{60}Co peak. Efficiency calibration was performed in both detectors using a polypropylene fiber filter as a blank in which aliquots of a standard solution of mixed radionuclides (R-08-04, National Laboratory of Physics, United Kingdom) supplemented with ^{210}Pb were homogeneously dispersed on the surface. The detectors are enclosed in 15 cm old iron-shields inside a clean laboratory. The laboratory is kept under positive pressure to minimize the concentration of radon in the indoor air. Each polypropylene filter was measured for 4 days, while blank filter measurements took 7 days. Gamma spectra analyses, including polypropylene blank filter correction, were performed with the Genie2K spectrometry software version 2.0 (Canberra Industries Inc., USA). A library of radionuclides, which contained the energy of the characteristic gamma peaks for each analyzed nuclide and their corresponding emission probabilities, was built from the data supplied in the mentioned software. The characteristic gamma peaks selected for the determination of the different radionuclides were: 477.59 keV for ^{7}Be, 1460.81 keV for ^{40}K, 46.54 keV for ^{210}Pb, and 661.65 keV for ^{137}Cs. The average Minimum Detectable Activity (MDA) for each studied radionuclide was (in mBq m^{-3}): 8.4×10^{-3} for ^{7}Be, 1.0×10^{-2} for ^{40}K, 1.8×10^{-2} for ^{210}Pb and 7.0×10^{-4} for ^{137}Cs. The activity concentrations of the radionuclides were corrected to account

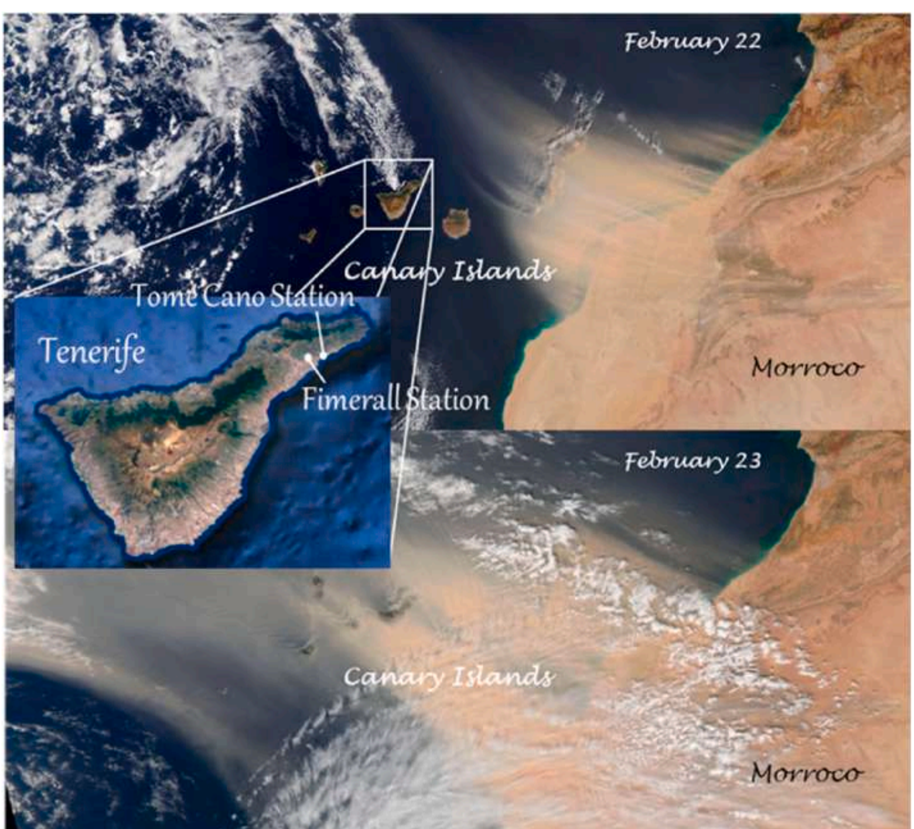

Fig. 1. Moderate Resolution Imaging Spectroradiometer (MODIS) NASA's Terra and Aqua satellites acquired during the dust storm on 22 and 23 February 2020. Inset shows Tenerife Island and the localization of the two stations used in this study.

for the decay after the collection date.

Gross alpha and gross beta activities in cellulose filters were measured with a multiple sample gas-flow proportional counter (Berthold LB770) 2 days after collection (to minimize the contribution of radon daughters). The calibration of each detector was performed by using planchets with a ^{241}Am activity of 27.2 Bq (alpha activity) and planchets of ^{90}Sr/^{90}Y with an activity of 100 Bq (beta activity). All gross alpha and gross beta activity calculations were corrected for the mass density of the aerosol deposit collected in the different filters. A self-absorption correction curve was previously built for this purpose from a series of samples spiked with a known activity of either ^{241}Am (for gross alpha) or ^{90}Sr + ^{90}Y (for gross beta) and increasing concentrations of sodium salt. The average detection limit of the low background proportional counter was 7.4×10^{-3} mBq m^{-3} and 1.6×10^{-2} mBq m^{-3} for alpha and beta activity, respectively. Due to the low concentration of alpha and beta emitters in the aerosol filter, a counting time of 36,000 s was used for each measurement. Cellulose blank filter measurements were carried out each week using similar counting times as for sample measurements. Blank filter subtraction procedure was applied to both gross alpha and gross beta analysis.

To validate the methods, our lab routinely participates in interlaboratory comparisons to measure gross alpha, gross beta and gamma-emitting radionuclides in air filters organized by the International Atomic Energy Agency (IAEA), the Joint Research Centre (JRC), and the Spanish Nuclear Safety Council (CSN). The z-score test was below 2 for all the tested radioactivity parameters, which indicates that the deployed method provided satisfactory results (Altzitzoglou et al., 2019; Máté et al., 2016).

To study the meteorology of this dust outbreak we used the fifth generation atmospheric reanalysis of the global climate data (ERA5), computed by the European Centre for Medium-Range Weather Forecasts (ECMWF) (Service_Copernicus_Climate_Change, 2017). The satellite images were obtained by the Spinning Enhanced Visible and Infra-Red Imager (SEVIRI) radiometer onboard on Meteosat Second Generation, whereas the aerosol optical depth (AOD) from the satellite was obtained by MODIS Adaptive Processing System (MODAPS), which uses the Moderate Resolution Imaging Spectroradiometer (MODIS) onboard Aqua and Terra satellites. All of this information is grouped on the NASA WorNASA_app, 2020ldview app (NASA_app, 2020).

To analyze the origin of the air mass that reached the Canaries in this episode we used 4-day isentropic back-trajectories computed by the Hysplit-4 model. To analyze the behavior of the air masses we chose three heights for the same final point: 300 m (the altitude of the FIMERALL stations), 1500 m, and 2800 m. Moreover, we did a geographic division concerning the area over the air masses flow. These sectors are chosen to take into account the sources of the aerosols and follow the criteria of (Díaz et al., 2006). For this dust storm, the movements of the air mass had a clear origin in the Saharan sector for any height.

For the in situ AOD we used the data obtained by a photometer CIMEL CE318 #424 situated at the University of La Laguna, very close to the FIMERALL stations (less than 5 km). This instrument belongs to the Spanish RIMA network, which is federated to the Aerosol Robotic Network (AERONET). As a member of this network, the instrument is calibrated each year for direct and diffuse solar measurements to assure the goodness of the data. The photometer measures the solar radiation at

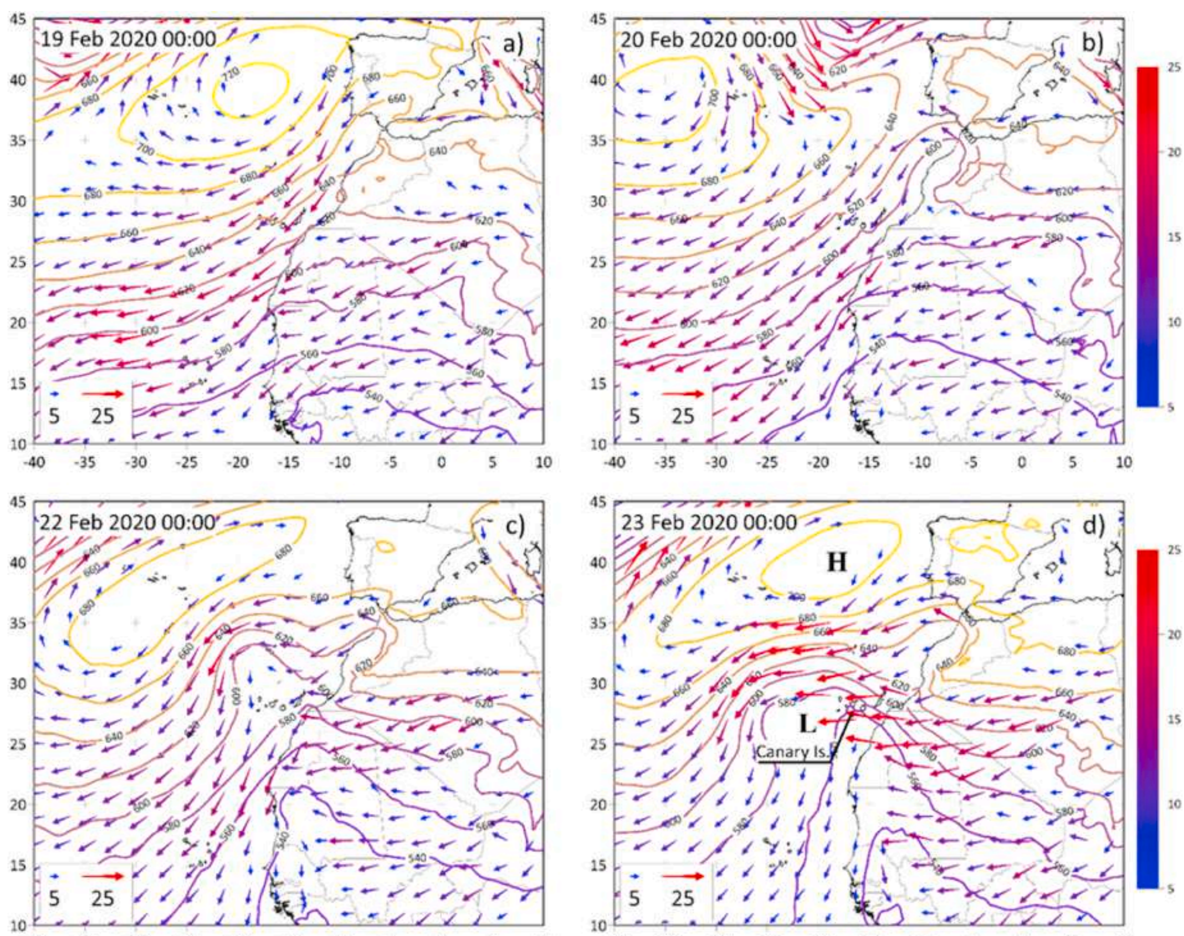

Fig. 2. Geopotential height (mgp) at 950 m and wind velocity (>5 m/s) maps using ERA5 data on February 19, 20, 22 and 23, 2020. Fig. 2 (d) shows the position of the cut-off low and the high close to the Canary Islands which produced a noticeable wind speed increase in this region.

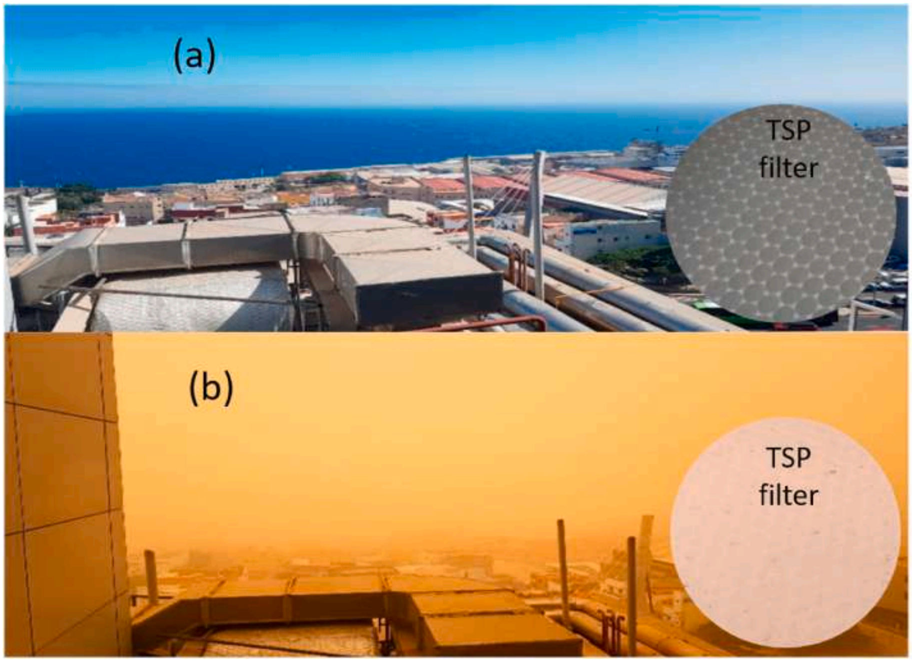

Fig. 3. Panoramic views of Santa Cruz de Tenerife, capital of Tenerife Island (situated 2 km from the FIMERALL stations), and appearance of filtering surfaces within the high-flow dust collector before (a) and during (b) the onset of the dust storm, respectively.

9 wavelengths from UV to NIR for daily sun elevation angles. Applying different algorithms, it is possible to obtain aerosol optical properties as AOD or spectral discrimination of coarse and fine mode optical depth (Dubovik and King, 2000; O'Neill et al., 2003).

Publicly available PM10 concentrations (μg m^{-3}) data were obtained from Tome Cano monitoring station located at Santa Cruz de Tenerife (Tome Cano station; 28°27′43.83″ N; 16°15′42.82″W, 67 m.a.s.l.), as part of the Air Quality Control and Surveillance Monitoring Network belonging to the Government of the Canary Islands. PM10 data were aggregated over periods of 7 days and average values were computed to fit the radiometric sampling period.

Statistical studies were obtained using the R program (Team_R_Core, 2020). Principal Component Analysis (PCA) and Cluster Analysis were applied using psych (v1.9.12.31) and factoextra (1.0.6) R packages respectively. To assess the sources of radionuclides in aerosol samples, PCA was applied to the weekly dataset. PCA is a multivariate technique that allows for transforming several possibly correlated variables into a smaller number of new variables called principal components (PCs) (Kaniu et al., 2018; Kumar et al., 2012; Sivakumar et al., 2014). Such PCs are linear combinations of the original ones, orthogonal and uncorrelated to each other. Therefore, PCA can be used to reduce the dimensionality of our data while controlling the loss of variance, projecting our dataset into a lower linear embedding space. PCA has been successfully applied in many fields of science such as geology, meteorology, astronomy, climatology, chemistry, biology, genetics, etc. Before PCA, data were conveniently normalized and centered.

Rotation techniques such as Varimax, Quartimax, Oblimin, etc., yield an increase of the weights of higher loadings and a reduction of lower ones, allowing an easier interpretation of the results (Jolliffe, 2002). The choice of the number of significant rotated PCs can be made following various criteria. In this work, rotated-PCs (RCs) were obtained applying the Varimax algorithm (Sivakumar et al., 2014) and retained when their eigenvalues were larger than unity as suggested by Kaiser's criteria (Kaiser, 1960). Finally, the rotated factor matrix, score and loading plots for the correct interpretation of the results were used. In addition, K-means and biplot methods were used for the correct group segmentation.

3. Results and discussions

3.1. Correlation analysis

Weekly variations of PM10, TSP mass collected in the two monitoring stations, gross alpha and gross beta activities, and ^{210}Pb, ^{7}Be, ^{137}Cs, and ^{40}K activity concentrations in atmospheric aerosols were measured corresponding to the sampling period from 1 July 2019 to 6 April 2020 (41 weeks).

Assuming a normal distribution, the linear dependence of the TSP data, obtained with the two different monitoring stations, against the weekly PM10 concentration was studied. The high Pearson's correlation coefficient of about 0.98 showed a high linear dependence of the TSP values with the PM10 concentration at Tome Cano station. Interestingly, the TSP registered in monitoring stations revealed the occurrence of other dust intrusion episodes previous to the main dust storm. For example, the low-flow station detected an increase in the TSP of 828% (85.6 mg) levels measured in cellulose filter related to the dust event recorded in early February (the week from 02/03/2020 to 02/10/2020) compared to the average value from July to December 2019. Moreover, the more sensitive high-flow station recorded an additional event in early January 2020 too. Such events can be clearly identified in Fig. 4.

Table 1 summarizes the results obtained during the dust storm and the average values calculated from the data collected in aerosol samples from July 2019 to December 2019 as well as for the period 2 March 2020 to 6 April 2020. TSP values registered after the dust storm show a noticeable mass increment when are compared with the mean value of previous weeks. The observed excursions in TSP levels represent an increment of 849% and 1778% for the high- and low-flow stations, respectively. Fig. 3 shows the filter loading under air clean conditions and the sampling filter obtained after the impact of the dust storm. The remarkably high levels of suspended particulate and the very low visibility associated with the dust intrusion provide an indication of the potential impact of the dust storm on air quality and health-related issues. The maximum hourly PM10 matter concentration measured in Santa Cruz de Tenerife was 2900 μg m^{-3}.Similarly to the maximum values registered during the same weekend (from 22 to 24, February) in Gran Canaria (3200 μg m^{-3}) and higher than those registered in other

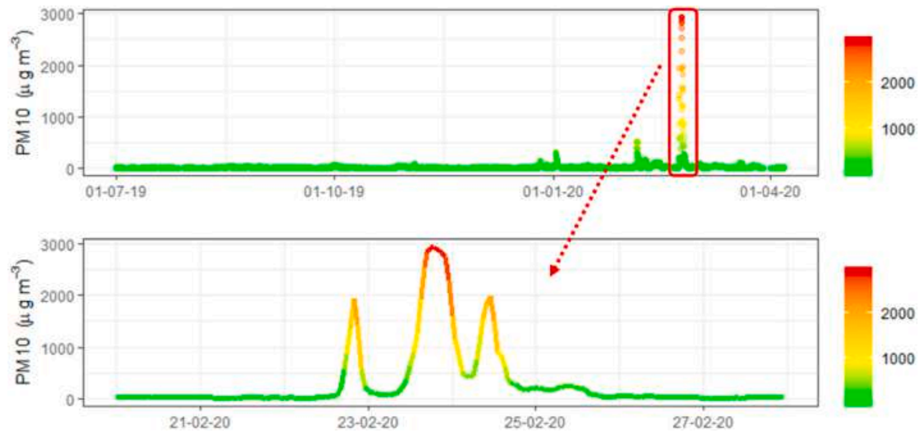

Fig. 4. Hourly variations of PM10 at Tome Cano monitoring station in atmospheric aerosol samples from 1 July 2019 to 6 April 2020. The largest peak, with values of about 3000 μg m^{-3}, depicts the arrival of the dust storm to the Canary Islands on February 23, 2020.

Table 1
Total Suspended Particulates (TSP), gross alpha, gross beta, ^{7}Be, ^{210}Pb, ^{40}K and ^{137}Cs activities measured in atmospheric aerosols collected in the low- and high-flow stations during the occurrence of the dust storm; and averaged values for two different periods.

		Dust Storm (A)		1 July 2019 to 30 December 2019 (B)		2 March 2020 to 6 April 2020 (C)		Ratio A/B (%)	Ratio A/C (%)
FIMERALL Station	Parameter	Value	Uncertainty	Mean value	Standard deviation	Mean value	Standard deviation		
Low-flow	TSP (g)	1900E-4	5E-4	11E-3	4E-3	10E-3	4E-3	1778	1900
	Gross alpha (mBq m^{-3})	57E-2	6E-2	7070E-5	6E-5	6E-2	3E-2	802	917
	Gross beta (mBq m^{-3})	105.0E-2	1.5E-2	6.4E-1	2.4E-1	4.4E-1	1.3E-1	164	238
High-flow	TSP (g)	2590.0E-2	1.1E-2	30E-1	8E-1	3.5E+0	1.0E+0	849	736
	^{7}Be (mBq m^{-3})	59.0E-1	1.1E-1	4.6E+0	1.3E+0	50E-1	8E-1	130	119
	^{210}Pb (mBq m^{-3})	66.1E-2	2.2E-2	6E-1	3E-1	5.3E-1	1.7E-1	112	125
	^{40}K (mBq m^{-3})	165E-3	4E-3	15E-3	6E-3	12.8E-3	1.3E-3	1068	1289
	^{137}Cs (mBq m^{-3})	22E-04	3E-4	<6.87E-4	N.A.	<5.57E-4	N.A.	316[a]	390[a]

N.A.: not applicable.
[a] Considering MDA mean value.

islands such as El Hierro (1000 μg m^{-3}), Lanzarote (969 μg m^{-3}) and Fuerteventura islands (941 μg m^{-3}) (Air_Quality).

This level of particles concentration can be also seen in the photometric measurements. The CIMEL photometer data (Fig. 5 and Fig. 6) clearly show the increase in the aerosol optical depth (AOD) at the beginning of this dust storm on 22 February with values ranging from 0.1 for 500 nm channel at the first hours of the day (typical values for this station) to 0.3 at 16:00.

Moreover, it is notorious the coarse mode of the particles as the main cause of this increase and the reduction in the Angström exponent (AE). This magnitude permits to parameterize the size of the atmospheric aerosols and has been widely used to distinguish between the presence of dust (low values of AE: 0.1–0.4) from clean situations (Carretas et al., 2015; Habib et al., 2019; Toledano et al., 2007; Valenzuela et al., 2015). Both measurements (high AOD and low AE) indicate the increase in the size of the aerosol that reaches the station. The next days, the 23 and 24 of February, the values of AOD were so high that the automatic filters applied to data consider they are clouds instead of dust. On February 25 the AOD values started to reduce although big particles were dominant yet. AOD data from the MODIS sensor onboard Aqua and Terra satellites and true-color images from SEVIRI (Meteosat satellite) showed how the dust cloud reached the Canary Islands on February 22 (Fig. 7). At the time of the satellite pass, the dust had reached the easterly islands of the archipelago.

The analysis of back-trajectories at low levels for these days indicates a clear origin in the Sahara Desert. As an example, Fig. 8 shows the back-trajectories at 3 heights, 300 m, 1500 m, and 2800 m for the noon of 23 February 2020 as the day of arrival. The trajectories which reach the Canaries in 4 days, cross the desert through the center of Algeria, dragging all the suspended particulate matter of the desert to heights below 2000 m, regardless of their final arrival altitude.

In addition, gross alpha, ^{40}K and ^{137}Cs activities increased over their overall average values (calculated from July to December 2019) by 802%, 1068%, and 316%, respectively (see Table 1). The activity concentration of ^{40}K was measured above the detection limits for 14 different weeks and ^{137}Cs concentration always was below the MDA during the period 1 July to 30 December 2019. On the contrary, gross beta, ^{7}Be, and ^{210}Pb activity concentrations did not show a noticeable increment of their values. Such findings suggest that gross alpha, ^{40}K, and ^{137}Cs activities are highly influenced by dust intrusions and might be used as proxies of the intensity of these episodes. As observed in Table 1, similar increments were obtained when such ratios (A/B and A/C) are calculated with the period from 2 March to 6 April 2020. ^{137}Cs was below the MDA during these weeks and ^{40}K was measured above the MDA only 1 week.

Pearson's correlations between measured radionuclides and PM10 concentrations were determined to study their collinearities. Table 2 shows the matrix of Pearson's correlation coefficients of gross alpha, gross beta, ^{40}K, ^{137}Cs, ^{7}Be and ^{210}Pb data measured in the atmospheric aerosol samples collected weekly from 1 July 2019 to 6 April 2020. Also, the PM10 concentrations measured in Tome Cano air quality monitoring station has been included in this analysis. The larger correlations

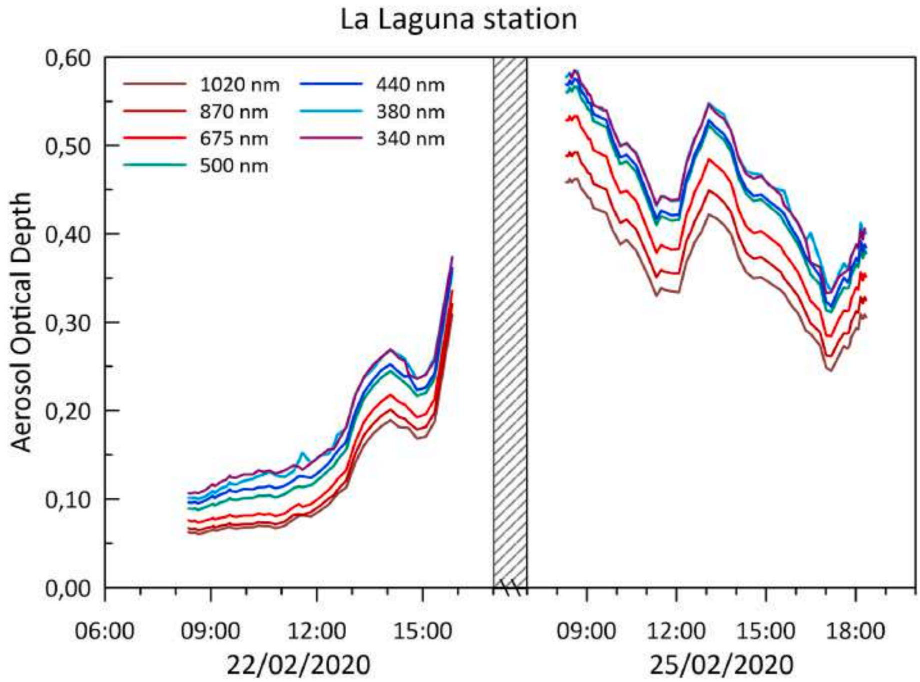

Fig. 5. *Aerosol optical depth (AOD) at the wavelengths of the CIMEL photometer #424 situated at La Laguna, Tenerife, during the days before and after the dust storm.*

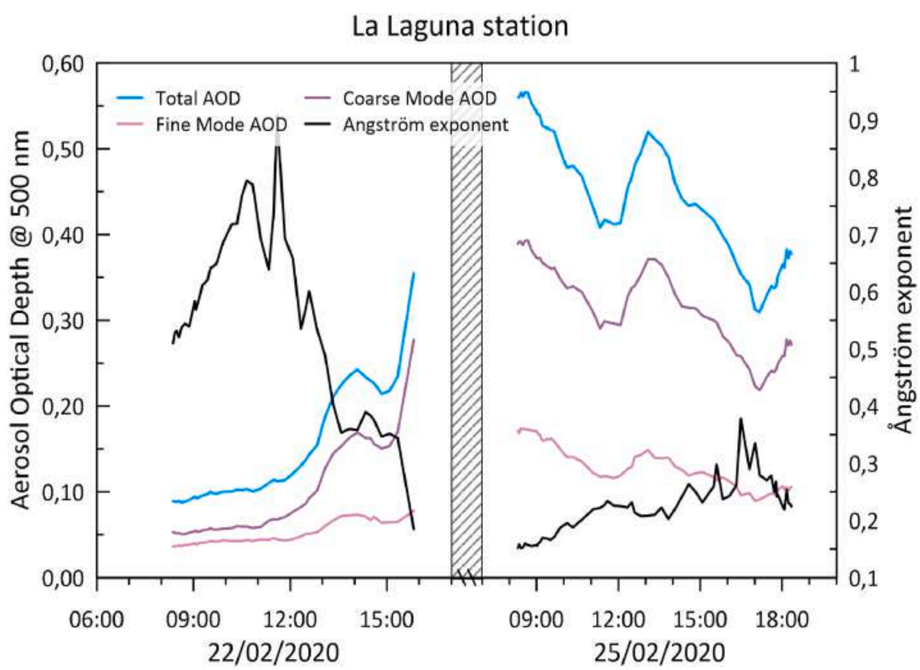

Fig. 6. Total aerosol optical depth (AOD) at 500 nm with its fine and coarse mode and Angström exponent during the days before and after the massive dust storm. The data were obtained by the CIMEL photometer #424 situated at La Laguna, Tenerife.

($>$0.80) were observed among PM10 concentration, gross alpha, ^{40}K and ^{137}Cs activities. This result points out that dust intrusions might be the main source of alpha emitters, ^{40}K and ^{137}Cs in the aerosol samples, as well as for TSP (as described above). On the contrary, gross beta, ^{7}Be and ^{210}Pb showed a low correlation with PM10 concentration. Moreover, low correlations were observed between ^{137}Cs and ^{210}Pb, and ^{137}Cs and ^{7}Be. ^{7}Be and ^{210}Pb showed a moderate positive correlation, suggesting that despite both radionuclides have different sources (cosmic and terrestrial origins, respectively) the dynamics in the low atmosphere of alpha and beta emitters contained within the aerosols was the same. Finally, the relatively high correlation between gross beta and ^{210}Pb activities suggests that ^{210}Pb is the main source for gross beta emitters in aerosol samples.

3.2. Temporal evolution

Fig. 9 and Fig. 10 show the weekly variations of PM10, TSP mass collected in the two monitoring stations, gross alpha and gross beta activities, and ^{210}Pb, ^{7}Be, ^{137}Cs and ^{40}K activity concentrations in atmospheric aerosols from 1 July 2019 to 6 April 2020. A dashed blue line

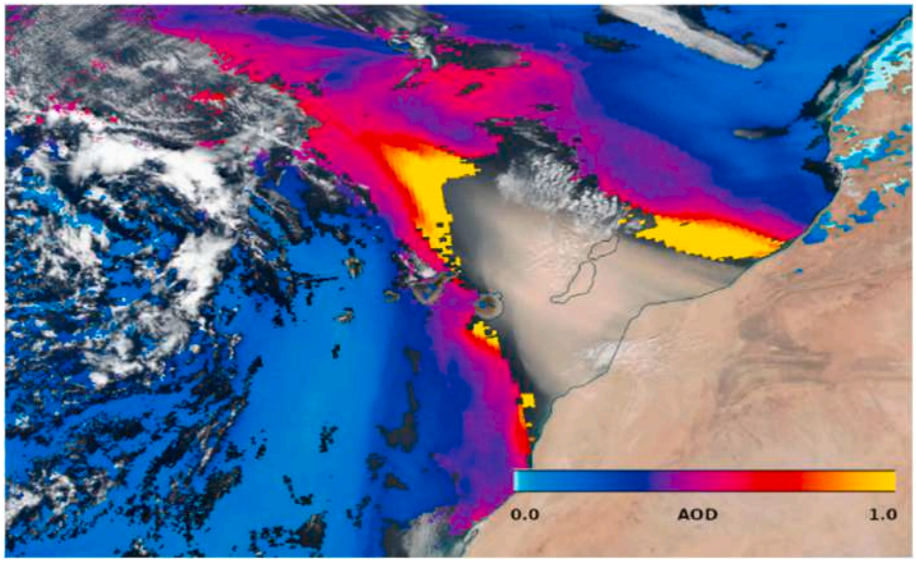

Fig. 7. Aerosol optical depth (AOD) obtained by the MODIS radiometer onboard Terra and Aqua satellites on 22 February 2020. The true-color image corresponds to the sensor SEVIRI of Meteosat satellite. (For interpretation of the references to color in this figure legend, the reader is referred to the Web version of this article.)

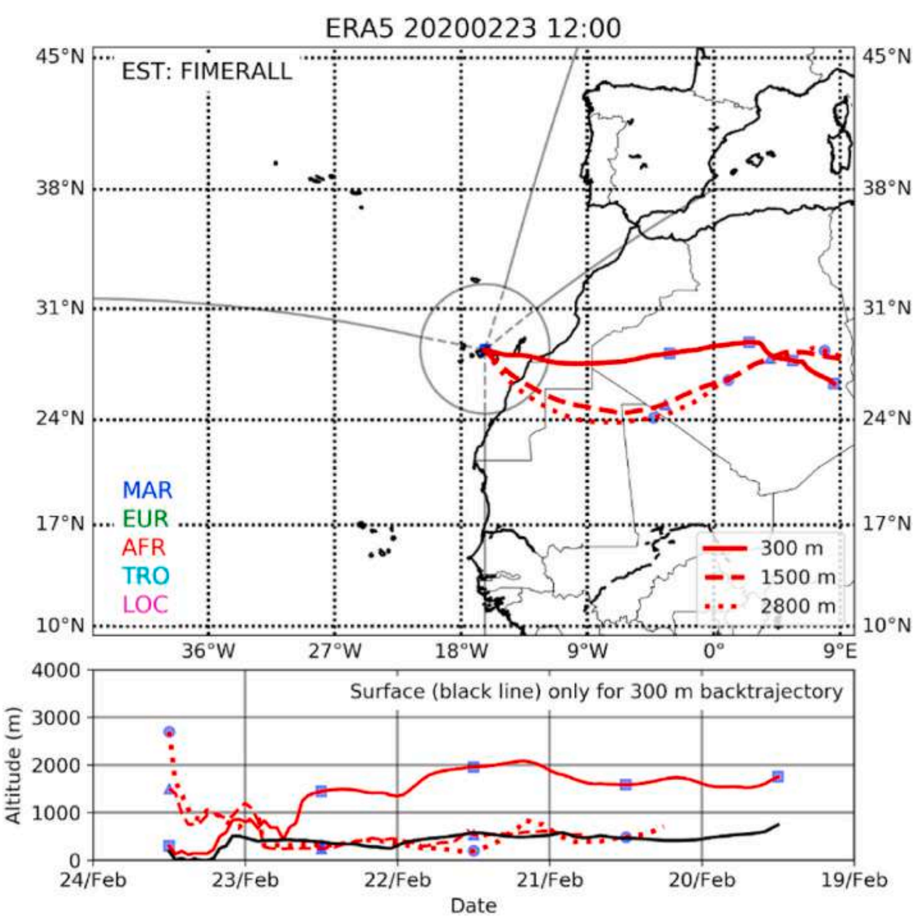

Fig. 8. Four-day back-trajectories for day 23 February 2020 reaching the Canary Islands at several heights: 300, 1,500, and 2800 m.a.s.l. (solid, dashed and dotted lines, respectively). Abbreviations with colors (in the left-down margin) reflect the region through which the air masses flow: Maritime (MAR), European (EUR), African (AFR), Tropical (TRO) and Local (LOC). (For interpretation of the references to color in this figure legend, the reader is referred to the Web version of this article.)

corresponds to the largest peak of dust intrusion caused during the dust storm on February 23, 2020.

Gross alpha activity (Fig. 9) correlates with dust intrusions episodes, and especially during the dust storm. However, gross beta activity levels did not show a similar correlation pattern with dust intrusions during the studied period. Such finding agrees with the correlation analysis reported above. Interestingly, gross alpha activity concentration showed a local maximum in early September 2019 (2–9 September), without an evident correlation with PM10 concentration in air (see Fig. 9). Based on these overall results, we hypothesize that a secondary alpha activity emitter source and/or a different mechanism of reaching the lower atmosphere at Tenerife Island occurred during this period.

Table 2
Pearson's correlation analysis of PM10 *concentrations and activity concentration of* ^{40}*K,* ^{137}*Cs,* ^{7}*Be,* ^{210}*Pb, gross alpha, and gross beta in aerosol samples* ($p < 0.05$).

	^{40}K	^{137}Cs	Gross alpha	PM10	^{7}Be	^{210}Pb	Gross beta
^{40}K	0	**0.97**	**0.83**	**0.89**	0.16	0.15	0.15
^{137}Cs		1	**0.92**	**0.85**	0.17	0.19	0.39
Gross alpha			1	0.89	0.29	0.3	**0.45**
PM10				1	0.14	0.2	0.34
^{7}Be					1	**0.42**	0.37
^{210}Pb						1	**0.71**
Gross beta							1

^{40}K and ^{137}Cs radionuclides showed higher activity values from January to March 2020, well correlated with dust intrusion episodes, especially with the arrival of the dust storm (see Fig. 10). This finding agrees with previous studies that indicated that those radionuclides can be used as radiotracers for African dust intrusions (Hernández et al., 2005b; Karlsson et al., 2008). Moreover, the higher values for both radionuclides during the January–February 2020 period are in good agreement with previous works, evidencing that the Saharan dust events occur at low altitudes during these months (Díaz et al., 2019; Viana et al., 2002). It is worthwhile to stress that ^{137}Cs activity was always below the MDA during the studied period, and has only been detected during the described dust intrusion events (for details see below). On the contrary, ^{210}Pb and ^{7}Be activities did not show any significant change

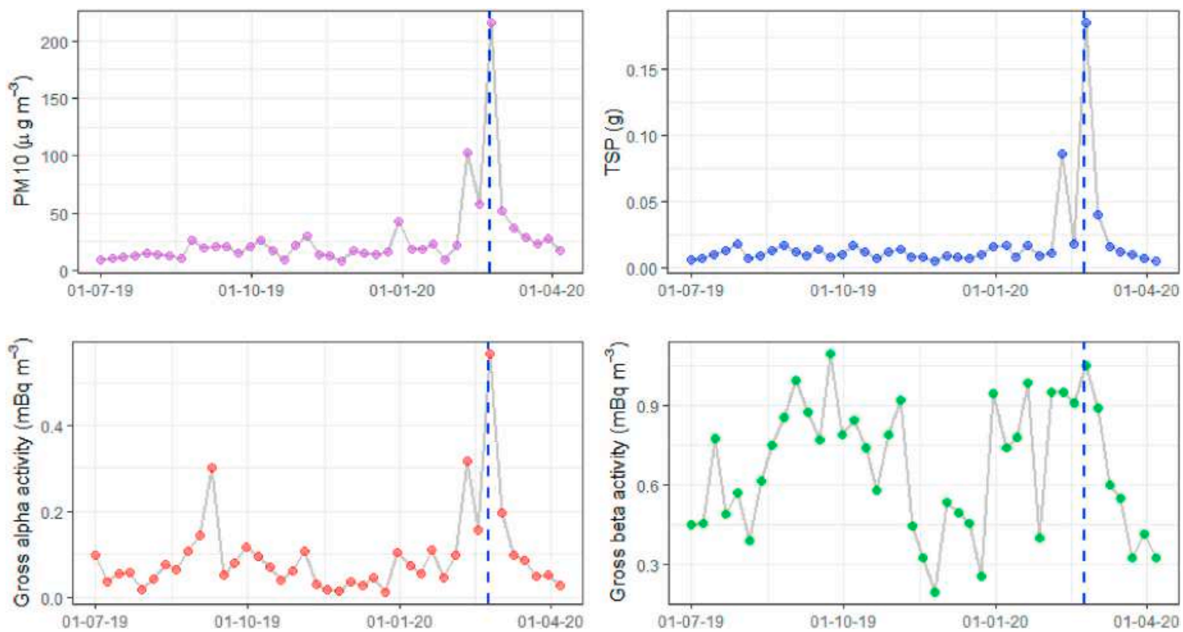

Fig. 9. *Weekly variations of* PM10 *at Tome Cano monitoring station, Total Suspended Particulates (TSP), gross alpha and gross beta activities in atmospheric aerosol samples measured in the low-flow station collected from 1 July 2019 to 6 April 2020. The dashed blue line depicts the arrival of the dust storm to the Canary Islands on February 23, 2020.* (For interpretation of the references to color in this figure legend, the reader is referred to the Web version of this article.)

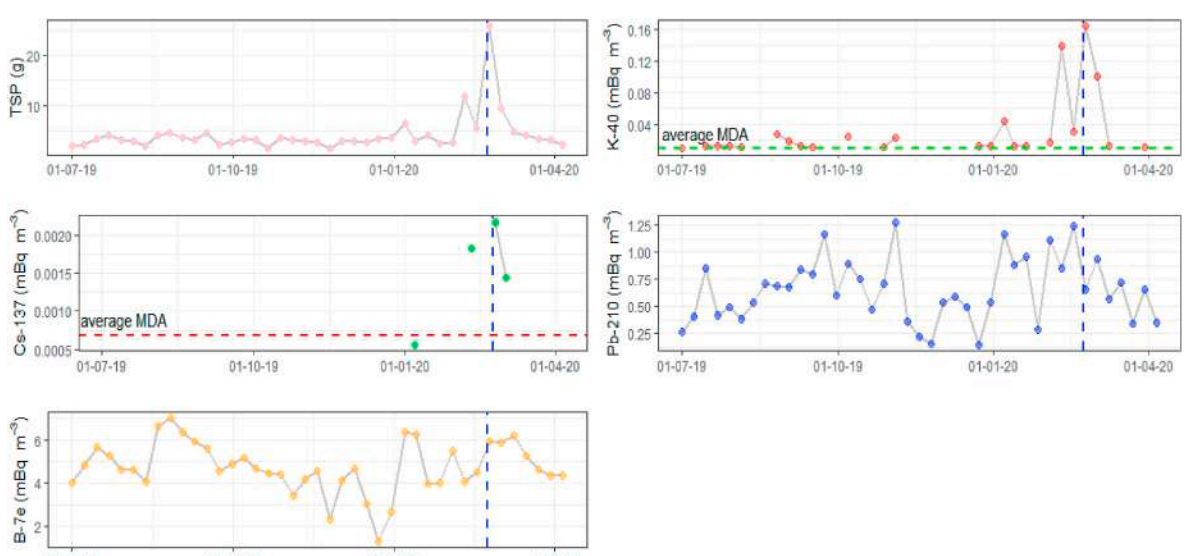

Fig. 10. Weekly variations of Total Suspended Particulates (TSP), ^{40}K, ^{137}Cs, ^{210}Pb and ^{7}Be activities at the high-flow station in atmospheric aerosol samples collected from 1 July 2019 to 6 April 2020. The dashed blue line depicts the arrival of the dust storm to the Canary Islands on February 23, 2020. (For interpretation of the references to color in this figure legend, the reader is referred to the Web version of this article.)

during the storm.

3.3. Principal Component Analysis

Results obtained for the rotated factor loadings for each variable are presented in Table 3. According to Kaiser's criteria, two main components with the largest eigenvalues of 4.00 and 1.67 were selected. The first two dimensions represented the ca. 81% of the total dataset variance. The first rotated component (RC1) explained ca. 51% of the total variance. Values for RC1 listed in Table 3 illustrate a positive correlation with ^{40}K (0.96), ^{137}Cs (0.96), gross alpha (0.88), and PM10 concentration (0.95). The second rotated component (RC2) explained 30% of the total variance and is determined by high positive loadings with ^{7}Be (0.67), ^{210}Pb (0.88), and gross beta (0.86).

Based on the nature of the variables that compose RC1, and on our previous works (Hernández et al., 2005b; Karlsson et al., 2008), we suggest that RC1 represents the Saharan contribution in our dataset. In addition, RC1 shows a high correlation with ^{40}K, ^{137}Cs, gross alpha, and PM10 variables that have previously been correlated with air masses in the MBL with a Northwestern African origin. The second component, representing gross beta, ^{7}Be, and ^{210}Pb radionuclides, may be interpreted as a mixed component that might be related to other air masses in the MBL (North Atlantic and Europe contributions).

K-means cluster analysis applied to the rotated dataset reveals the existence of three different clusters (see Fig. 11) that could indicate differences in the origin of the air masses arriving at Tenerife Island. The first identified cluster (Continental) corresponds to weeks with high values of gross beta, ^{210}Pb, and ^{7}Be activity concentrations. Such cluster represents the ca. 49% of the weeks sampled during this study and may be related to continental air masses from different origins (Europe and Africa) and patterns. The second cluster (Oceanic) represents the ca. 44% of the analyzed weeks and is characterized by low values of PM10 air concentrations, gross beta, gross alpha, and ^{210}Pb, ^{7}Be, and ^{40}K activity concentrations. Such a cluster is assigned to Atlantic air contributions with lower radionuclides and microparticulate matter. The last group, identified as Calima cluster (dust intrusion contribution), is characterized with high PM10 values and ^{137}Cs, ^{40}K and gross alpha activity concentrations, and represent ca. 7% of the total analyzed period.

Back-trajectories for some weeks from the three clusters (Oceanic, Continental and Calima) were randomly selected to confirm their correct identification. Back-trajectories for nine well-identified weeks are shown in Fig. 12 (three for each cluster, for details see Fig. 11). Weeks (4, 22 and 26) grouped in the Oceanic cluster showed an important marine contribution with a clear NNW Atlantic origin of the air masses. Interestingly week number 4, with an intermediate position in the biplot representation (nearby the Continental cluster), showed an origin closer to the Iberian Peninsula that may produce mixing processes between European and marine contributions. All weeks (12, 15 and 29) grouped in the Continental cluster showed a clear NNE origin (European origin) with some mixing contribution during week number 15 with marine

Table 3
Results of the Varimax rotated factor matrix (loadings > 0.6 are marked in bold).

	RC1	RC2
^{7}Be	0.11	**0.67**
^{210}Pb	−0.09	**0.88**
^{40}K	**0.96**	0.16
^{137}Cs	**0.96**	0.04
Gross alpha	**0.88**	0.32
Gross beta	0.19	**0.86**
PM10	**0.95**	0.16
Eigenvalue	4.00	1.67
Variance explained	0.51	0.30
Total variance explained	0.51	0.81

RC = Rotated Component.

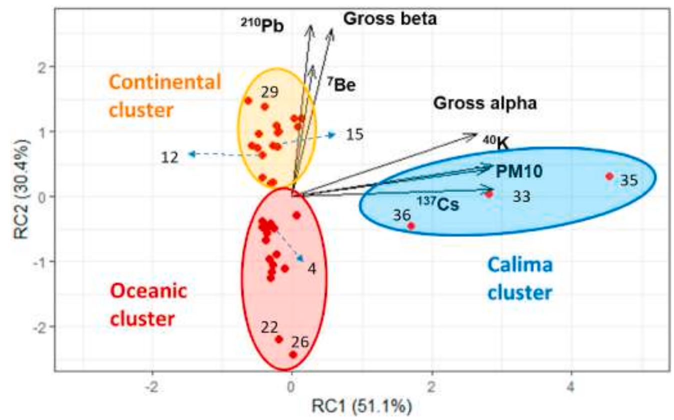

Fig. 11. Biplot and K-means clusters obtained after Varimax rotation, for details see Table 3. Numbers within the figure represent selected weeks whose back-trajectories are shown in Fig. 12.

contribution. Finally, the three weeks (33, 35 and 36) grouped in the Calima cluster, corresponded with dust intrusions registered in the Canary Islands. Their back-trajectories confirmed the important contribution of African air masses from the Sahara Desert during these weeks.

4. Conclusions

In this study, we have assessed the impact of a strong dust storm affecting the Canary Islands archipelago (Spain) on 22–24 February 2020. Measurements of several natural and artificial radionuclides (^{40}K, ^{137}Cs, ^{210}Pb, ^{7}Be), and gross alpha and gross beta activity concentrations were performed on atmospheric aerosols. The findings described here have shown strong evidence of the correlation between the mass of total suspended matter, PM10, and ^{40}K and ^{137}Cs activity concentrations. ^{40}K and ^{137}Cs showed activity values over the MDA from January to March 2020, coupled with the arrival of several dust intrusions from Africa.

Gross beta and ^{210}Pb activities showed a high correlation suggesting that ^{210}Pb is the main source for gross beta emitters in the collected aerosol samples. ^{210}Pb and ^{7}Be showed a moderate positive correlation and did not show any significant change during the main storm in February 2020, suggesting a similar dynamics of alpha and beta emitters within the low atmosphere layer at the latitude of the Canary Islands.

A Principal Component Analysis of these observations showed two components representing a Saharan component (grouping ^{40}K, ^{137}Cs, gross alpha, and PM10) and a heterogeneous component representing North Atlantic and Europe air masses (grouping ^{7}Be, ^{210}Pb, and gross beta). Additionally, a K-means cluster analysis lets us disentangle the putative origin of air masses arriving at the archipelago. Three distinct clusters were identified: a Continental cluster (gross beta, ^{210}Pb, and ^{7}Be activity concentrations); an Oceanic cluster (with low values of PM10 air concentrations, gross beta, gross alpha, and ^{210}Pb, and ^{7}Be and ^{40}K activity concentrations), reflecting the Atlantic air contributions with lower radionuclide activity and microparticulate matter; and a dust intrusion cluster (with high PM10 values and ^{137}Cs, ^{40}K and gross alpha activity concentrations) representing dust intrusion episodes observed in Tenerife Island.

These findings support the use of some of the studied radionuclides as radiotracers for African low altitude dust intrusions occurring particularly during the winter over the Canary Islands. These studies allow the detection and monitoring of radioactive elements, estimating the potential radiological risk to the population associated with mineral dust intrusions.

Author contribution statements

M. López-Pérez, P. Salazar and J.M. Lorenzo-Salazar conceived of the

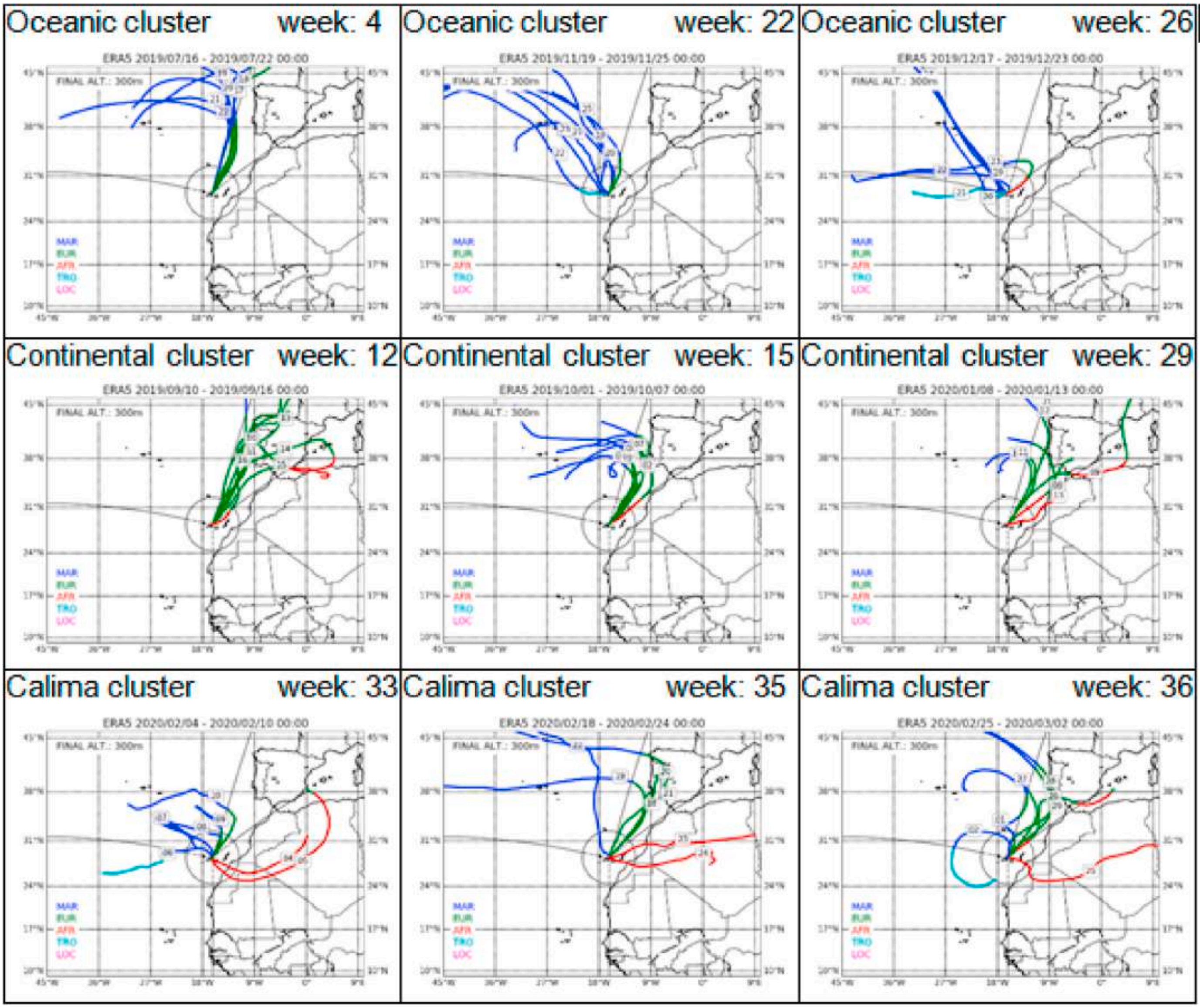

Fig. 12. Four-day back-trajectories (one simulation for each day) for three weeks (grouped in the Oceanic, Continental and Calima Clusters) reaching the Canary Islands at 300 m.a.s.l. Abbreviations with colors (in the left-down margin) reflect the region through which the air masses flow: Maritime (MAR), European (EUR), African (AFR), Tropical (TRO) and Local (LOC). (For interpretation of the references to color in this figure legend, the reader is referred to the Web version of this article.)

presented study. M. López developed the analytical measurements. F.J. Expósito and J.P. Díaz supervised and verified the atmospheric models and data. P. Salazar and J.M. Lorenzo-Salazar performed the statistical study and its interpretation. All authors discussed the results and contributed to the final manuscript.

Declaration of competing interest

The authors declare that they have no known competing financial interests or personal relationships that could have appeared to influence the work reported in this paper.

Acknowledgements

We wish to express our gratitude to the CSN (Consejo de Seguridad Nuclear) for their support to the Laboratory of Environmental Radioactivity of La Laguna University. We would also like to thank the Government of the Canary Islands for providing PM10 data at the Tome Cano monitoring station.

Authors thank Rubén García Martínez for the panoramic views of Santa Cruz de Tenerife from the Hospital Universitario Nuestra Señora de Candelaria.

The authors gratefully acknowledge the NOAA Air Resources Laboratory (ARL) for the provision of the HYSPLIT transport and dispersion model and/or READY website (https://www.ready.noaa.gov) used in this publication.

We also thank the meteorological data generated using Copernicus Climate Change Service Information [2020].

We acknowledge the use of imagery from the NASA Worldview application (https://worldview.earthdata.nasa.gov), part of the NASA Earth Observing System Data and Information System (EOSDIS).

The members of the Grupo de Observación de la Tierra y la Atmósfera thank to the PLANCLIMAC Project (MAC/3.5b/244) for its support. This Project is financed by the European Union INTERREG MAC 2014–2020 Program.

Appendix A. Supplementary data

Supplementary data to this article can be found online at https://doi.org/10.1016/j.atmosenv.2020.117806.

References

[ERROR!: PLEASE CHECK REFERENCE STYLE]2008/50/EC, 2008. Directive 2008/50/EC of the European Parliament and of the Council of 21 May 2008 On ambient air quality and cleaner air for Europe. Orkesterjournalen L 152, 1–44, 11.6.
[ERROR!: PLEASE CHECK REFERENCE STYLE]2008/50/EC, 2011. Establishing Guidelines for Demonstration and Subtraction of Exceedances Attributable to Natural Sources under the Directive 2008/50/EC on Ambient Air Quality and Cleaner Air for Europe, Brussels, 15.02. 2011. SEC(2011) 208 Final, p. 37.
AERONET. Aerosol robotic network (AERONET) homepage. https://aeronet.gsfc.nasa.gov.
Air_Quality. Air quality Control and surveillance monitoring network. Government of the Canary Islands. https://www3.gobiernodecanarias.org/medioambiente/calidaddelaire/inicio.do.
Alonso-Pérez, S., Cuevas, E., Querol, X., Viana, M., Guerra, J.C., 2007. Impact of the Saharan dust outbreaks on the ambient levels of total suspended particles (TSP) in the marine boundary layer (MBL) of the Subtropical Eastern North Atlantic Ocean. Atmos. Environ. 41, 9468–9480.
Altzitzoglou, T., Hult, M., De Cort, M., 2019. Evaluation of the 2016 ENV57 MetroERM measurement comparison on 137Cs, 134Cs and 131I in air filters. Appl. Radiat. Isot. 143, 123–131.
Andreae, M., Rosenfeld, D., 2008. Aerosol-cloud-precipitation interactions. Part 1. The nature and sources of cloud-active aerosols. Earth Sci. Rev. 13–41.
Baggoura, B., Noureddine, A., Benkrid, M., 1998. Level of natural and artificial radioactivity in Algeria. Appl. Radiat. Isot. 49, 867–873.
Baldasano, J.M., Soret, A., Guevara, M., Martínez, F., Gassó, S., 2014. Integrated assessment of air pollution using observations and modelling in Santa Cruz de Tenerife (Canary Islands). Sci. Total Environ. 473–474, 576–588.
Beuck, H., Quass, U., Klemm, O., Kuhlbusch, T.A.J., 2011. Assessment of sea salt and mineral dust contributions to PM10 in NW Germany using tracer models and positive matrix factorization. Atmos. Environ. 45, 5813–5821.
Bustos, J.J., Cuevas, E., Marrero, C., 1998. Caracterización de las masas de aire en la troposfera libre y en la capa de mezcla en Canarias. In: Proceedings of the IX Asamblea Geodesia Y Geofísica, Aguadulce (Almería), pp. 9–13.
Cardoso, J., Almeida, S.M., Nunes, T., Almeida-Silva, M., Cerqueira, M., Alves, C., Rocha, F., Chaves, P., Reis, M., Salvador, P., Artiñano, B., Pio, C., 2018. Source apportionment of atmospheric aerosol in a marine dusty environment by ionic/composition mass balance (IMB). Atmos. Chem. Phys. 18, 13215–13230.
Carretas, F., Wagner, F., Janeiro, F.M., 2015. Atmospheric visibility and Angström exponent measurements through digital photography. Measurement 64, 147–156.
Danesi, P.R., Moreno, J., Makarewicz, M., Louvat, D., 2008. Residual radionuclide concentrations and estimated radiation doses at the former French nuclear weapons test sites in Algeria. Appl. Radiat. Isot. 66, 1671–1674.
Díaz, A.M., Díaz, J.P., Expósito, F.J., Hernández-Leal, P.A., Savoie, D., Querol, X., 2006. Air masses and aerosols chemical components in the free troposphere at the subtropical northeast atlantic region. J. Atmos. Chem. 53, 63–90.
Díaz, J.P., Expósito, F.J., Pérez, J.C., González, A., Wang, Y., Haimberger, L., Wang, J., 2019. Long-term trends in marine boundary layer properties over the atlantic ocean. J. Clim. 32, 2991–3004.
Dubovik, O., King, M.D., 2000. A flexible inversion algorithm for retrieval of aerosol optical properties from Sun and sky radiance measurements. J. Geophys. Res.: Atmosphere 105, 20673–20696.
El_Día, 2020. El Cabildo aprueba una línea de ayudas para los daños agrícolas del temporal. https://www.eldia.es/tenerife/2020/03/06/tenerife-impulsa-ayudas-afectados-temporal/1058172.html.
El_País, 2020. La calima, el viento y el fuego cierran el espacio aéreo y marítimo en Canarias. https://elpais.com/politica/2020/02/23/actualidad/1582449863_096738.html.
Euronews, 2020. Canary Islands sandstorm from Sahara disrupts hundreds of flights. https://www.euronews.com/2020/02/24/massive-saharan-sandstorm-grounds-flights-in-canary-islands.
Gehlot, S., Minnett, P.J., Stammer, D., 2015. Impact of Sahara dust on solar radiation at Cape Verde Islands derived from MODIS and surface measurements. Rem. Sens. Environ. 166, 154–162.
Goudie, A.S., 2014. Desert dust and human health disorders. Environ. Int. 63, 101–113.
Goudie, A.S., Middleton, N.J., 2001. Saharan dust storms: nature and consequences. Earth Sci. Rev. 56, 179–204.
Habib, A., Chen, B., Khalid, B., Tan, S., Che, H., Mahmood, T., Shi, G., Butt, M.T., 2019. Estimation and inter-comparison of dust aerosols based on MODIS, MISR and AERONET retrievals over Asian desert regions. J. Environ. Sci. 76, 154–166.
Hernández, F., Alonso-Pérez, S., Hernández-Armas, J., Cuevas, E., Karlsson, L., Romero-Campos, P.M., 2005a. Influence of major African dust intrusions on the 137Cs and 40K activities in the lower atmosphere at the Island of Tenerife. Atmos. Environ. 39, 4111–4118.
Hernández, F., Hernández-Armas, J., Catalán, A., Fernández-Aldecoa, J.C., Karlsson, L., 2005b. Gross alpha, gross beta activities and gamma emitting radionuclides composition of airborne particulate samples in an oceanic island. Atmos. Environ. 39, 4057–4066.
Huneeus, N., Schulz, M., Balkanski, Y., Griesfeller, J., Prospero, J., Kinne, S., Bauer, S., Boucher, O., Chin, M., Dentener, F., Diehl, T., Easter, R., Fillmore, D., Ghan, S., Ginoux, P., Grini, A., Horowitz, L., Koch, D., Krol, M.C., Landing, W., Liu, X., Mahowald, N., Miller, R., Morcrette, J.J., Myhre, G., Penner, J., Perlwitz, J., Stier, P., Takemura, T., Zender, C.S., 2011. Global dust model intercomparison in AeroCom phase i. Atmos. Chem. Phys. 11, 7781–7816.
Jolliffe, 2002. Rotation and Interpretation of Principal Components, Principal Component Analysis. Springer New York, New York, NY, pp. 269–298.
Kaiser, H.F., 1960. The application of electronic computers to factor Analysis. Educ. Psychol. Meas. 20, 141–151.
Kaniu, M.I., Angeyo, K.H., Darby, I.G., 2018. Occurrence and multivariate exploratory analysis of the natural radioactivity anomaly in the south coastal region of Kenya. Radiat. Phys. Chem. 146, 34–41.
Karanasiou, A., Moreno, N., Moreno, T., Viana, M., de Leeuw, F., Querol, X., 2012. Health effects from Sahara dust episodes in Europe: literature review and research gaps. Environ. Int. 47, 107–114.
Karlsson, L., Hernandez, F., Rodríguez, S., López-Pérez, M., Hernandez-Armas, J., Alonso-Pérez, S., Cuevas, E., 2008. Using 137Cs and 40K to identify natural Saharan dust contributions to PM10 concentrations and air quality impairment in the Canary Islands. Atmos. Environ. 42, 7034–7042.
Krupke, A., Mohr, W., LaRoche, J., Fuchs, B.M., Amann, R.I., Kuypers, M.M.M., 2015. The effect of nutrients on carbon and nitrogen fixation by the UCYN-A-haptophyte symbiosis. ISME J. 9, 1635–1647.
Kumar, A., Joshi, V.M., Mishra, M.K., Karpe, R., Rout, S., Narayanan, U., Tripathi, R.M., Singh, J., Kumar, S., Hegde, A.G., Kushwaha, H.S., 2012. Distribution, enrichment and principal component analysis for possible sources of naturally occurring and anthropogenic radionuclides in the agricultural soil of Punjab state, India. Radiat. Protect. Dosim. 150, 71–81.
Masson, O., Piga, D., Gurriaran, R., D'Amico, D., 2010. Impact of an exceptional Saharan dust outbreak in France: PM10 and artificial radionuclides concentrations in air and in dust deposit. Atmos. Environ. 44, 2478–2486.
Máté, B., Sobiech-Matura, K., Altzitzoglou, T., 2016. Evaluation of the 2014 EC measurement comparison on 137Cs in air filters. Appl. Radiat. Isot. 109, 36–40.
Menut, L., Masson, O., Bessagnet, B., 2009. Contribution of Saharan dust on radionuclide aerosol activity levels in Europe? The 21–22 February 2004 case study. J. Geophys. Res.: Atmosphere 114.
Middleton, N.J., 2017. Desert dust hazards: a global review. Aeolian Res. 24, 53–63.
NASA_app, 2020. https://worldview.earthdata.nasa.gov.
O'Neill, N.T., Eck, T.F., Smirnov, A., Holben, B.N., Thulasiraman, S., 2003. Spectral discrimination of coarse and fine mode optical depth. J. Geophys. Res.: Atmosphere 108.
Okin, G.S., Baker, A.R., Tegen, I., Mahowald, N.M., Dentener, F.J., Duce, R.A., Galloway, J.N., Hunter, K., Kanakidou, M., Kubilay, N., Prospero, J.M., Sarin, M., Surapipith, V., Uematsu, M., Zhu, T., 2011. Impacts of atmospheric nutrient deposition on marine productivity: roles of nitrogen, phosphorus, and iron. Global Biogeochem. Cycles 25.
Perez, L., Tobías, A., Querol, X., Pey, J., Alastuey, A., Díaz, J., Sunyer, J., 2012. Saharan dust, particulate matter and cause-specific mortality: a case–crossover study in Barcelona (Spain). Environ. Int. 48, 150–155.
Prospero, J.M., 1999. Long-range transport of mineral dust in the global atmosphere: impact of African dust on the environment of the southeastern United States. Proc. Natl. Acad. Sci. U. S. A. 96, 3396–3403.
Prospero, J.M., Ginoux, P., Torres, O., Nicholson, S.E., Gill, T.E., 2002. Environmental characterization of global sources of atmospheric soil dust identified with the nimbus 7 total ozone mapping spectrometer (toms) absorbing aerosol product. Rev. Geophys. 40, 2–31.
Querol, X., Alastuey, A., Moreno, T., Viana, M.M., Castillo, S., Pey, J., Rodríguez, S., Artiñano, B., Salvador, P., Sánchez, M., Garcia Dos Santos, S., Herce Garraleta, M.D., Fernandez-Patier, R., Moreno-Grau, S., Negral, L., Minguillón, M.C., Monfort, E., Sanz, M.J., Palomo-Marín, R., Pinilla-Gil, E., Cuevas, E., de la Rosa, J., Sánchez de la Campa, A., 2008. Spatial and temporal variations in airborne particulate matter (PM10 and PM2.5) across Spain 1999–2005. Atmos. Environ. 42, 3964–3979.
Querol, X., Pérez, N., Reche, C., Ealo, M., Ripoll, A., Tur, J., Pandolfi, M., Pey, J., Salvador, P., Moreno, T., Alastuey, A., 2019a. African dust and air quality over Spain: is it only dust that matters? Sci. Total Environ. 686, 737–752.
Querol, X., Tobías, A., Pérez, N., Karanasiou, A., Amato, F., Stafoggia, M., Pérez García-Pando, C., Ginoux, P., Forastiere, F., Gumy, S., Mudu, P., Alastuey, A., 2019b. Monitoring the impact of desert dust outbreaks for air quality for health studies. Environ. Int. 130, 104867-104867.
Rodríguez, S., Guerra, J.C., 2001. Monitoring of ozone in a marine environment in Tenerife (canary islands). Atmos. Environ. 35, 1829–1841.
Schweitzer, M.D., Calzadilla, A.S., Salamo, O., Sharifi, A., Kumar, N., Holt, G., Campos, M., Mirsaeidi, M., 2018. Lung health in era of climate change and dust storms. Environ. Res. 163, 36–42.
Service_Copernicus_Climate_Change, 2017. ERA5: fifth generation of ECMWF atmospheric reanalyses of the global climate. Copernicus climate change Service climate data store (CDS). https://cds.climate.copernicus.eu/cdsapp#!/home.
Sivakumar, S., Chandrasekaran, A., Ravisankar, R., Ravikumar, S.M., Prince Prakash Jebakumar, J., Vijayagopal, P., Vijayalakshmi, I., Jose, M.T., 2014. Measurement of natural radioactivity and evaluation of radiation hazards in coastal sediments of east coast of Tamilnadu using statistical approach. J. Taibah Univ. Sci. 8, 375–384.
Team_R_Core, 2020. R: a foundation for statistical computing, vienna, Austria (Vienna, Austria). https://www.R-project.org/.
The_Washington_Post, 2020. Canary Islands sandstorm grounds flights, closes schools as Sahara dust moves into open Atlantic. https://www.washingtonpost.com/weather/

2020/02/24/canary-islands-sandstorm-grounds-flights-closes-schools-sahara-dust-moves-into-open-atlantic/.
Toledano, C., Cachorro, V.E., de Frutos, A.M., Sorribas, M., Prats, N., de la Morena, B.A., 2007. Inventory of african desert dust events over the southwestern iberian Peninsula in 2000–2005 with an AERONET cimel sun photometer. J. Geophys. Res.: Atmosphere 112.
Torres, C.J., Cuevas, E., Guerra, J.C., Carreño, V., 2001. Caracterización de las Masas de Aire en la Región Subtropical, Instituto ed (Madrid).
Valenzuela, A., Olmo, F.J., Lyamani, H., Antón, M., Titos, G., Cazorla, A., Alados-Arboledas, L., 2015. Aerosol scattering and absorption Angström exponents as indicators of dust and dust-free days over Granada (Spain). Atmos. Res. 154, 1–13.
Viana, M., Querol, X., Alastuey, A., Cuevas, E., Rodríguez, S., 2002. Influence of African dust on the levels of atmospheric particulates in the Canary Islands air quality network. Atmos. Environ. 36, 5861–5875.
Weger, M., Heinold, B., Engler, C., Schumann, U., Seifert, A., Fößig, R., Voigt, C., Baars, H., Blahak, U., Borrmann, S., Hoose, C., Kaufmann, S., Krämer, M., Seifert, P., Senf, F., Schneider, J., Tegen, I., 2018. The impact of mineral dust on cloud formation during the Saharan dust event in April 2014 over Europe. Atmos. Chem. Phys. 18, 17545–17572.
WHO, 2006. Air Quality Guidelines Global Update 2005. Particulate Matter, Ozone, Nitrogen Dioxide and Sulfur Dioxide, ISBN 92 890 2192 6.
WHO, 2013. Review of Evidence on Health Aspects of Air Pollution - REVIHAAP Project. Technical Report, Copenhagen, Denmark.
Zhang, H., Gu, W., Li, Y.J., Tang, M., 2020. Hygroscopic properties of sodium and potassium salts as related to saline mineral dusts and sea salt aerosols. J. Environ. Sci. 95, 65–72.